Chemiluminescent reactions of rare gas atoms, Rg(ns, 3P2, 3P1, 1P1) with N2O, SCO and SeCO: Spectroscopy and energy disposal in rare gas oxide, sulphide and selenide excimers

ARTICLE *in* CHEMICAL PHYSICS LETTERS · JUNE 1987

Impact Factor: 1.9 · DOI: 10.1016/0009-2614(87)80206-3

4 AUTHORS, INCLUDING:

Agust Kvaran
University of Iceland
87 PUBLICATIONS **1,116** CITATIONS
SEE PROFILE

John P Simons
University of Oxford
297 PUBLICATIONS **6,700** CITATIONS
SEE PROFILE

CHEMILUMINESCENT REACTIONS OF RARE GAS ATOMS, Rg(ns, $^3P_2$, $^3P_1$, $^1P_1$) WITH N_2O, SCO AND SeCO: SPECTROSCOPY AND ENERGY DISPOSAL IN RARE GAS OXIDE, SULPHIDE AND SELENIDE EXCIMERS

Agust KVARAN [1], AUDUNN LUDVIKSSON
Science Intitute, University of Iceland, Dunhaga 3, 107 Reykjavik, Iceland

William S. HARTREE and J.P. SIMONS
Chemistry Department, The University, Nottingham NG7 2RD, UK

Received 20 February 1987; in final form 21 March 1987

Chemiluminescence associated with excimer states of XeO, KrO, ArO, XeS and XeSe has been generated through the reaction of electronically excited rare gas atoms, Rg(ns, $^3P_2$, $^3P_1$, or $^1P_1$) with N_2O, SCO, SCNH or SeCO. Branching ratios into the atom-transfer channels for reactions of Rg($^3P_2$) are $< 1\%$. Experiments using a superthermal reagent beam of Xe($^3P_2$) indicate translational threshold behaviour for the reaction $Xe(^3P_2)+N_2O\rightarrow(Xe^+O^-)^*+N_2$. Estimates of the initial vibrational population distributions and spectroscopic parameters of XeO and KrO have been achieved through a preliminary analysis of their chemiluminescence spectra.

1. Introduction

UV or VUV chemiluminescence spectra attributed to ion-pair states in rare gas oxides were first reported in 1974 but the observations were neglected in the excitement generated by the simultaneous report of chemiluminescence from the rare gas halides [1] and the rapid development of excimer lasers. In both cases the fluorescence transfers the carrier from a bound ion-pair state onto repulsive or weakly attractive lower-lying neutral potentials. The neutral atom-pair states correlating with O, S or Se(^1S) also have potential as laser storage media [2–4].

Recently interest in the oxide and sulphide excimers has been revived by Setser and co-workers [5] and by ourselves [6] following the discovery, and rediscovery, of their fully dispersed chemiluminescence spectra excited through reaction of $Xe[6p(1/2)]_0$ or $Xe[6p(3/2)]_2$ [5] or Xe, Kr, $Ar[6s(3/2)]_{2,1}$ or $Xe[6s(1/2)]_1$ [6] with N_2O and SCO. Setser's group reported a kinetic study of the generation and quenching of the excimer fluorescence from XeO and XeS [5]. The present work describes a complementary study of XeO, KrO, ArO, XeS and XeSe with emphasis on spectral analysis and vibrational energy disposal in the nascent excimer.

2. Experimental techniques

Energy-resolved, digitised UV and VUV chemiluminescence spectra were recorded using techniques described earlier [7–9]. Spectra excited through reactions of Xe, Kr and $Ar(^3P_{2,0})$ with N_2O were generated in a discharge flow system; chemiluminescent reactions of Xe($^3P_1$ or $^1P_1$) with N_2O, SCO, SCNH or SeCO were promoted through absorption of Xe resonance radiation at 147 nm and/or 129.5 nm passed through a BaF_2 or LiF window. The spectral intensities from the fluorescence of XeO and KrO were analysed by spectral simulation [10,11] or direct inversion [12]. The excitation function for the reaction

$$Xe(^3P_2)+N_2O\rightarrow XeO^*\rightarrow N_2 \qquad (1)$$

[1] To whom correspondence should be addressed.

0 009-2614/87/$ 03.50

was determined under superthermal atomic beam–Maxwellian target gas conditions at 300 K, over the c.m. collision energy range 6–46 kJ mol^{-1} using a rotor accelerated atomic beam source [7].

3. Results

3.1. N_2O

Fig. 1 shows the UV and VUV chemiluminescence spectra excited by reaction of $Xe(^3P_2)$, $Kr(^3P_2)$ or $Ar(^2P_{2,0})$ with N_2O. The main feature in each case is an unstructured bound-to-free continuum lying at the short-wavelength limit of the spectrum, and analogous with the B→X system in the rare gas halides. The continua have peak intensities at 235 nm (XeO), 180 nm (KrO) and 150 nm (ArO) and have been attributed to emission from the ion-pair excimer state(s) Rg^+O^- into the repulsive ground-state potential $X\,^3\Pi$ correlating with $Rg(^1S_0)+O(^3P_J)$ [5,6]. The excimer emission of XeO has also been excited, albeit weakly, by irradiation of Xe/N_2O mixtures with resonance radiation at 147 nm (exciting $Xe(^3P_1)$) and more strongly by replacing the BaF_2 window with LiF to allow transmission of the resonance line at 129.5 nm. The increased intensity implies a major increase in the branching ratio for atom transfer to $Xe(^1P_1)$ compared with $Xe(^3P_1)$. An increased contribution from the emission observed in the short-wavelength tail of the continuum also suggests an enhanced level of vibrational excitation in the XeO generated by $Xe(^1P_1)$.

Branching ratios, $\Gamma(RgO)$ for generation of the rare gas oxide excimers have been estimated by comparing the fluorescence intensities excited through reaction of Xe, $Kr(^3P_2)$ with N_2O, with those of RgCl(B) excited by the corresponding reactions with Cl_2. Combining these data with the rate constants for the total quenching of Xe, $Kr(^3P_2)$ by N_2O [11,13–15] we derive the branching ratios listed in table 1. The atom transfer channels are seen to be minor for the $^3P_2$ states. However, this is not the case for the more highly excited states: Setser and coworkers find that substitution of $Xe[6p(1/2)]_0$ or $Xe[6p(3/2)]_2$ for $Xe(^3P_2)$ increases $\Gamma(XeO)$ to about 0.1 [5]; the branching ratio for $Xe(6s, {}^1P_1)$ is probably of the same order. The spectra shown in fig. 1 display many additional features lying to the red of the main continuum. Those for the $Xe(^3P_2)/N_2O$ and $Kr(^3P_2)/N_2O$ systems are all tentatively assigned to emission from the excimer state(s) of XeO, KrO into the neutral atom-pair states correlating with $O(^3P)$ or $O(^1D)$ (see figs. 1 and 2). Their justification is presented in section 4. The interaction of $Kr(^3P_2)$ and N_2O also excites emissions from $N_2(B\,^3\Pi_g)$ [13], while $Ar(^3P_{2,0})$ excites emission from $N_2(B\,^3\Pi_g, a\,^1\Pi_g, a\,^1\Sigma_u^-)$, $NO(B\,^2\Pi)$ and $O(^5S, {}^3S)$ [1,13,14]. The atomic emission may well reflect predissociation of the ArO excimer.

Substitution of SCO, SCNH or SeCO for N_2O leads to a new series of chemiluminescence spectra when their mixtures with Xe are exposed to radiation at 129.5 nm: fig. 1d shows the emission spectrum excited in Xe/SCO. No emissions could be detected when the resonance radiation was filtered through a BaF_2 window ($Xe(^3P_1)$) or through reaction of $Xe(^3P_2)$ under discharge flow conditions. Thermochemical estimates indicate that the reactions of $Xe(^3P_2, {}^3P_1)$ are endothermic (see section 4).

The spectral contour of the chemiluminescence excited in the Xe/SCO mixtures closely mirrors that of the XeO emission. The main continuum peaking at 225 nm has been attributed to the transition from the excimer XeS, into the atom-pair ground state [5] while the weaker features lying to longer wavelengths are again tentatively assigned to transitions terminating on the excited atom-pair ground state [5] while the weaker features lying to longer wavelengths are again tentatively assigned to transitions terminating on the excited atom-pair potentials correlating with $S(^3P_J, {}^1D_2)$. An identical spectrum was excited when SCNH was substituted for SCO reinforcing the assignment to XeS and a similar emission was generated by reaction of $Xe(^1P_1)$ with SeCO; the principal band peaked at 218 nm and was attributed to the excimer XeSe.

3.2. Analysis of the principal excimer bands: vibrational energy disposals in the rare gas oxides

The spectral profiles of the main continua excited in each of the rare gas/N_2O systems closely resembles those observed for the rare gas halide excimers when their vibrational population distributions are relatively relaxed and uninverted [1,5–7]. Determina-

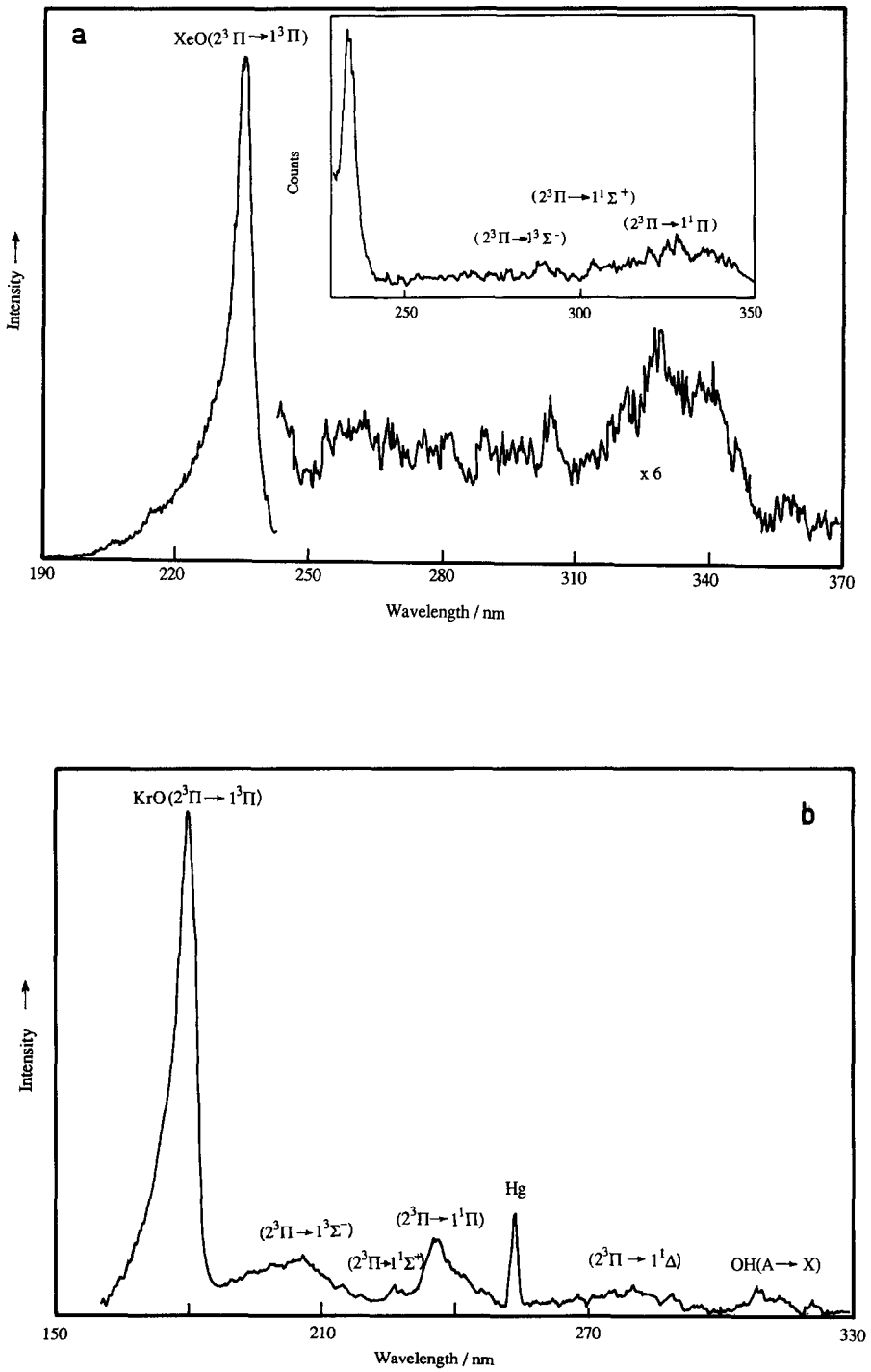

Fig. 1. Chemiluminescence spectra excited by reaction of N_2O with (a) Xe($^3P_2$ and $^3P_1$); (b) Kr($^3P_{2,0}$); (c) Ar($^3P_{2,0}$); (d) of SCO with Xe($^1P_1$). Total pressures 1 Torr in all cases: spectra shown in (a–c) have been corrected for spectral response.

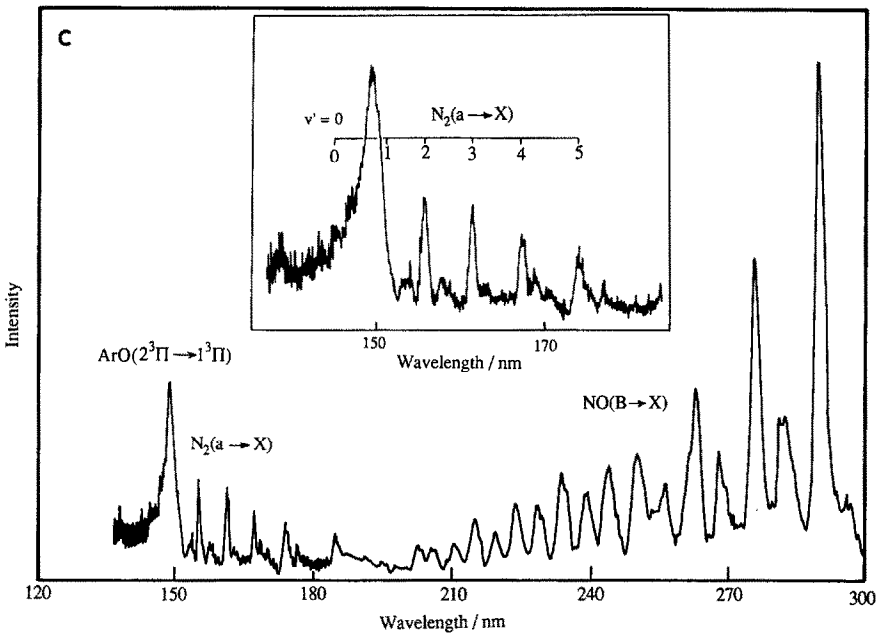

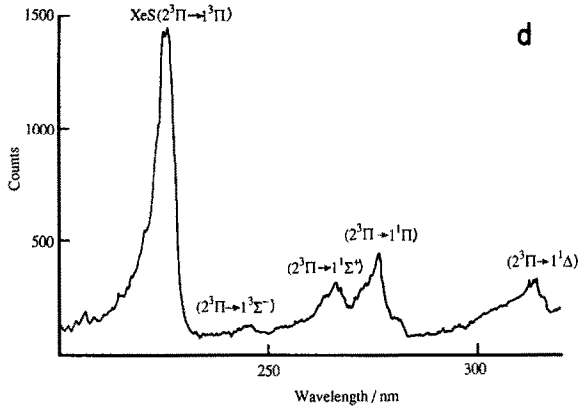

Fig. 1. Continued.

tion of the vibrational population distributions via direct spectral inversion requires accurate data for the upper and lower potentials and the transition moment functions. Unfortunately, these are not all available so in order to effect at least an approximate analysis a compromise strategy was adopted.

Table 1
Rate constants, $k(RgO)$; branching fractions, $\Gamma(RgO)$, and vibrational energy disposals, $\langle f_{v'} \rangle$ in the reactions $Rg^* + N_2O \rightarrow RgO + N_2$

	$Xe(^3P_2)/N_2O$	$Kr(^3P_2)/N_2O$	$Ar(^3P_{2,0})/N_2O$	$Xe(^1P_1)/N_2O$
$k(RgO)$ ($cm^3\ s^{-1}$)	1.4×10^{-12} [a]	3×10^{-12} [a]	$<2\times10^{-12}$ [a]	
$\Gamma(RgO)$	0.003	0.010	<0.005 [a]	
v'_{max}	29 ± 7	25 ± 9	-	72 ± 10
$\langle f_i \rangle$	≈0.25	≈0.27	-	≈0.17

[a] Ref. [14].

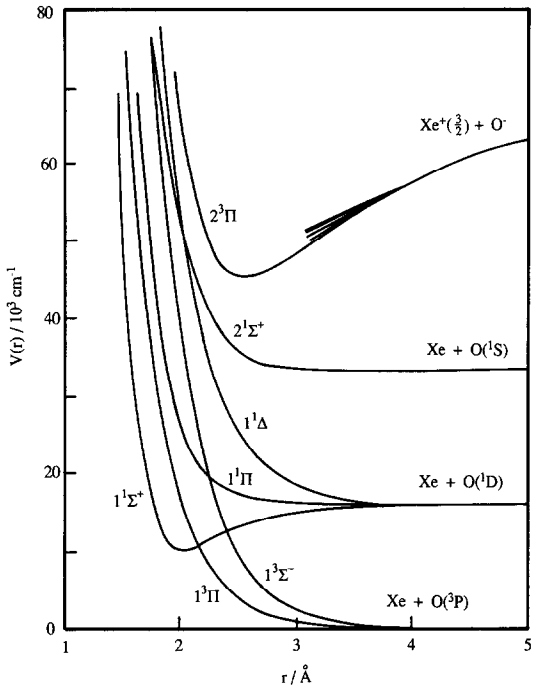

Fig. 2. Potential curves for XeO (from ref. [16] and this work).

The vibrational populations were assumed to approximate either a Boltzmann distribution, represented by a temperature parameter T_v, or a linear surprisal distribution [8,11] represented by a parameter λ_v. Either one of the parameters was first employed as an adjustable variable, to be used in spectral simulation calculations; when an acceptable agreement between experiment and simulation was achieved by simultaneous variation of the potential parameters, the optimised potentials were used in a direct inversion of the experimental spectra to obtain final optimised vibrational population distributions.

In the absence of experimentally determined potentials for the rare gas oxides, the ion-pair states were represented by the function

$$U'(r) = a' \exp(-r/b') - c_1'/r + d' , \qquad (2)$$

while the atom-pair potentials $U''(r)$ were represented by the functions

$$U''(r) = a'' \exp(-r/b'') - c_6''/r^6 \qquad (3)$$

fitted to the ab initio calculations of Langhoff [16]. The parameters a' and b' are constrained by the requirement that the chosen potentials match the positions of the experimental spectra; $d' =$ IP(Rg) − EA(O): table 2 lists the optimised parameter sets finally employed in the inversion procedure. The transition moments, assumed to be decreasing functions of the internuclear distance by analogy with equivalent electronic transitions in the rare gas halides [17], were represented by the function

$$\mu(r) = \left(\sum_i c_i (r + r_0)^i \right)^{-1} \exp[-\gamma(r + r_0 - a)]. \qquad (4)$$

Table 2
Parameters for the excimer and ground-state atom-pair potentials (in cm^{-1}) $U(r) = a \exp(-r/b) - c_1/r - c_6/r^6 + d$

	a (10^{-7} cm^{-1})	b (Å)	c_1 (10^{-5} Å cm^{-1})	c_6 (10^{-5} $Å^6$ cm^{-1})	d (10^{-5} cm^{-1})
XeO(2 $^3\Pi$)	10.5419	0.2571	1.1606	0	0.8628
KrO(2 $^3\Pi$)	2.3352	0.2924	1.1606	0	1.0213
XeO(1 $^3\Pi$)	1.0602	0.3131	0	0	0
KrO(1 $^3\Pi$)	1.3938	0.2953	0	1.41	0

Table 3
Variation of transition moment, μ, as a function of internuclear distance $\mu(r) = [\Sigma_i c_i (r + r_0)^i]^{-1} \exp[-\gamma(r + r_0 - a)]$

	c_0	c_1	c_2	c_3	c_4	γ (Å)	a (Å)	r_0 (Å)
XeO	20.95	−21.22	8.20	−1.43	0.098	0.5	3.585	1.02
KrO	20.95	−21.22	8.20	−1.43	0.098	1.1	3.585	1.15

The parameters c_i were selected by analogy with the corresponding rare gas halides [9,11,12], while γ was varied as an adjustable parameter (see table 3).

We now consider the optimisation procedures using XeO as our example. Variation of the potential parameters a' and b' leads to a variation of the vibrational frequency ω_e' and equilibrium distance r_e' associated with the upper state potential. The

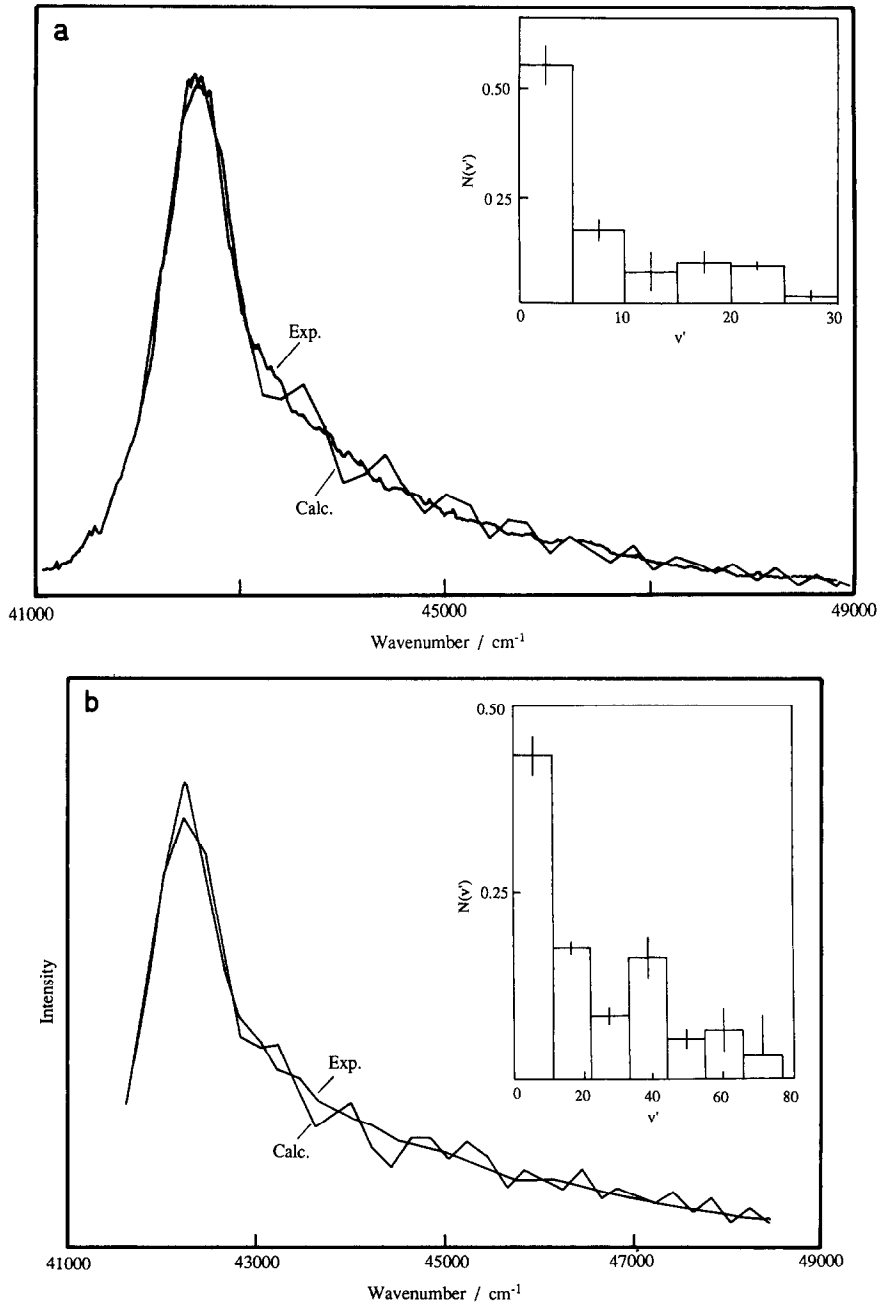

Fig. 3. Vibrational population distributions in XeO($2\,^3\Pi$) determined by direct inversion of the experimental spectra shown in fig. 2, using the optimised parameters listed in tables 2, 3 and 5. (a) Xe($^3P_2$), (b) Xe($^1P_1$).

spectroscopic parameters ω'_e and r'_e were optimised by determining rms values for the difference between the calculated and experimental spectral intensities at 200 cm^{-1} intervals, for alternative choices of ω'_e/r'_e, transition moment parameters, μ, and vibrational temperatures, $T_v = 2000$, 3000 and 4000 K to give the spectroscopic parameters ω'_e, r'_e and T'_e and the vibrational parameter T_v. The highest accessible vibrational level v'_{max} must satisfy the energy balance

$$T'_e + G_e(v'_{max}) = E(Rg^*) + \tfrac{5}{2}RT - D_0(N_2\text{–}O) \; . \qquad (5)$$

Fig. 3a shows the "goodness-of-fit" with the optimised choice of parameters. These were finally employed in a direct inversion of the experimental spectrum to obtain the steady state vibrational population histogram. (The influence of rotational excitation was ignored in most of the simulation calculations: for $J < 100$ there was no significant change in the spectral contours beyond a slight shift in the oscillatory structure.) Not surprisingly(!) the vibrational surprisal parameter λ_v was close to zero. The spectroscopic parameters were also used to invert the spectrum excited by reaction of $Xe(^3P_1, {}^1P_1)$ with N_2O. The result, shown in fig. 3b reinforces the view that the reactive state is principally $Xe(^1P_1)$ since the considerably increased maximum level of vibrational excitation, $v'_{max} = 72 \pm 10$, cf. 29 ± 7 correlates closely with the increased available energy $E(^1P_1\text{–}^3P_2)$.

The results obtained through a similar analysis of the KrO excimer emission band centred at 180 nm, excited by reaction of $Kr(^3P_2)$ with N_2O, are collected in tables 1, 2 and 3. Unfortunately, overlapping emission from $N_2(a\text{–}X)$ complicates analysis of the corresponding ArO excimer band, and the complete absence of *any* potential parameters for XeS precludes any analysis of its spectrum. However, the similarity in the spectral contours in each system encourages the view that the excimers are all generated with similarly shaped vibrational population distributions.

4. Discussion

4.1. Energy requirements and energy disposal

Exoergicities, ΔE_0 for the atom transfer reactions

Table 4
Exo(endo)ergicities ΔE_0 (cm^{-1}), for the generation of RgX* (estimated from the frequencies of the excimer band)

	N_2O	SCO	SeCO
$Xe(^3P_2)$	-7070 ± 360	$\leqslant +6470$	$\leqslant +4500$
$Xe(^1P_1)$	–	$\leqslant -3660$	$\leqslant -5630$
$Kr(^3P_2)$	-5770 ± 460	–	–
$Ar(^3P_2)$	-9000	–	–

$Rg^* + N_2O$ can be estimated using eq. (5), and the term values T'_e listed in tables 2 and 3 (or estimated from the energy of the excimer band in the case of ArO) (see table 4). Estimates of ΔE_0 for the reactions with SCO or SeCO are necessarily approximate, since the excimer band maxima only provide a lower limit for T'_e. However, estimates made on this basis clearly indicate that the reactions of $Rg(^3P_2)$ are strongly endoergic, while $Xe(^1P_1)$ has sufficient excitation to overcome the barrier. Despite the exoergicity of the reactions with N_2O, the cross section for production of XeO through collision of $Xe(^3P_2)$ with N_2O increases steadily with the collision energy (see fig. 4). In view of the low electron affinity of N_2O, $(EA)_{ad} \approx 0.2$ eV [18], and the consequent short range of the covalent–ionic potential surface intersection, some repulsion in the entrance channel might be expected [19] – assuming reaction proceeds via a harpoon mechanism. The statistically distributed and low levels of vibrational energy dis-

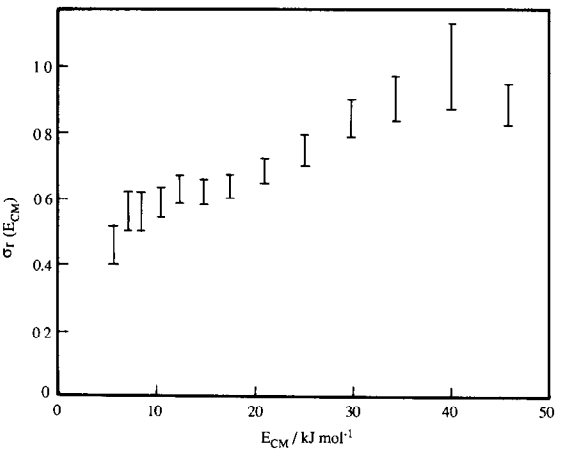

Fig. 4. Excitation function for the generation of XeO chemiluminescence from the reaction of $Xe(^3P_2)$ with N_2O at 295 K.

posal in the XeO and KrO excimers encourages the suggestion of a long-lived reactive collision complex. A reduced level of vibrational excitation imposed by predissociation of XeO can be excluded in view of the increased excitation promoted by $Xe(^1P_1)$.

4.2. Comparisons with MO and RgX

Table 5 compares the estimated values of r'_e and ω'_e for the emitting excimer state of XeO and KrO with the corresponding data for the alkali metal oxides, fluorides, and the rare gas halides. A comparison is also made with the well depths, D'_e. In all cases, the self-consistency of the estimates is gratifying in the light of the approximations and assumptions employed in the analysis. Many ion-pair states may be generated by the association of $Rg^+(^2P_{3/2,1/2})$ with $O^-(^2P_{3/2,1/2})$; the large spin–orbit splitting in Xe, Kr and Ar would divide these into two clusters. In practice, no excimer emission bands have been detected at wavelengths shorter than the principal band, suggesting either the absence of the higher cluster or its rapid predissociation. The splittings *within* each cluster would be very small and, to the extent that the "singlet/triplet" designations are appropriate, the data can be interpreted in favour of a single emitting state, designated $2\,^3\Pi$ [5].

4.3. Spectral assignments

The bands peaking at 270, 292 and 330 nm (XeO) and 245, 266 and 278 nm (XeS) have all been assigned by Setser and co-workers to emission from the $^3\Pi$ excimer state into excited atom-pair potentials [5]; they have also observed the perturbed auroral band associated with the transition $2\,^1\Sigma^+(O(^1S)) \rightarrow 1\,^1\Sigma^+(O(^1D))$ [5]. Our own analysis which is based on the frequency differences with respect to the main band, differs slightly from theirs, and is summarised in table 6. The features at 330/340 nm (XeO), 235 nm (KrO) and 276 nm (XeS) all correlate closely with the asymptote associated with $O(^1D)$ or $S(^1D)$ and are assigned to the transition $2\,^3\Pi \rightarrow 1\,^1\Pi$ (cf. fig. 3). The features at 292 nm (XeO), 225 nm (KrO) and 266 nm (XeS) each lie at energies which quantitatively reflect the expected stabilisation associated with the attractive character of the $1\,^1\Sigma^+$ potential [16]. Any emission into the highest neutral potential, $2\,^1\Sigma^+$ should lie at much longer wavelengths.

4.4. Laser implications

The rare gas oxide, sulphide and selenide excimers may well extend the family of excimer laser media. Their $2\,^3\Pi \rightarrow 1\,^3\Pi$ radiative lifetimes are of the same order as those for the rare gas halides (B→X) and they can be generated in electrical discharges [5]. Predissociation of the $2\,^3\Pi$ state(s) does not appear to present problems, at least in the xenon excimers and in KrO, though there could be difficulties associated with slow vibrational relaxation. Increasing the pressure of Ar as a buffer gas, in the $Xe(^3P_J)/N_2O$ systems, promotes only a barely perceptible narrowing in the band at 235 nm in marked contrast to the very fast relaxation in the rare gas halides [8,23]. On the other hand, if the nascent rare gas oxides, etc., are generated with low vibrational excitation, slow

Table 5
Comparison of the spectroscopic contants of XeO and KrO with those of the alkali metal oxides, fluorides and rare gas halides

	ω_e (cm^{-1})	r_e (Å)	T_e (cm^{-1})	D_e (cm^{-1})	Ref.
XeO	360±20	2.59±0.04	45920±350	40358	this work
XeF	303	2.68		40895	[20]
CsO	(314)	2.47–2.50			[21]
CsF	352	2.345			[22]
KrO	365±25	2.43±0.06	60100±450	42534	this work
KrF	339	2.51		42830	[20]
RbO	433	2.28			[21]
RbF	376	2.27			[22]

Table 6
Suggested assignments of XeO*, KrO* and XeS* excimer emission bands

Terminating state		λ_{max} (nm)	ν_{max} (cm^{-1})	A (cm^{-1})	$A+U''(r'_e)$ (cm^{-1})
$1\,^3\Pi$	XeO	235	42550	0	2775
	KrO	180	55555	0	3035
	XeS	225	44640	0	800
$1\,^3\Sigma$	XeO	270	37040	5510	8285
	KrO	207	48310	7245	10280
	XeS	245	40820	3820	4620
$1\,^1\Sigma^+$	XeO	292	34250	8300	11075 [a]
	KrO	225	44440	11110	14145 [a]
	XeS	266	37590	7050	7850 [b]
$1\,^1\Pi$	XeO	330	30300	12250	15025
		339	29500	13050	15825 cf. $E(O(^1D))=15868$
	KrO	235	42550	13005	16040
	XeS	276	36230	8410	9210 [b] cf. $E(S(^1D))=9234$
$1\,^1\Delta$	KrO	280	35715	19840	22875
	XeS	335	29850	14790	15590

[a] Reflecting stabilisation energies with respect to the $Rg+O(^1D)$ asymptotes $\approx 4800\,cm^{-1}$ (XeO) and $\approx 700\,cm^{-1}$ (KrO) at $r_e(RgO^*)$.
[b] Estimates based on assignment of XeS band at 276 nm to $2\,^3\Pi \rightarrow 1\,^1\Pi$.

relaxation rates may not present a serious problem. In any case relaxation might be greatly accelerated by the addition of a molecular buffer gas. The low branching fraction for rare gas oxide formation need not be a constraint since the mechanism in a discharge would most likely involve ionic rather than neutral reagents. The commercial XeCl laser produces an interesting comparison; lasing is induced by discharge of Xe/HCl mixtures although XeCl formation is endothermic for reaction of $Xe(^3P_2)$ [9].

5. Conclusion

A proper spectroscopic analysis of the new family of rare gas excimers must await accurate "ab initio" potentials. It is hoped these will not be long delayed in view of relevance to the development of alternative laser systems. Enough is known, however, to encourage further spectroscopic and molecular beam studies, which may generate improved spectral data both for the excimer states and the manifold of atom-pair potentials and promote a better understanding of the dynamics of the excimer producing reactions.

Acknowledgement

We are grateful for the support of the Icelandic University Research Foundation and a NATO Collaborative Award (Grant No. 0315/83). We also thank Thorgeir E. Thorgeirsson for assistance in the measurements of RgO branching ratios.

References

[1] M.F. Golde and B.A. Thrush, Chem. Phys. Letters 29 (1974) 486.
[2] W.M. Hughes, N.T. Olson and R. Hunter, Appl. Phys. Letters 28 (1976) 81.
[3] H.T. Powell, J.R. Murray and C.K. Rhodes, Appl. Phys. Letters 25 (1974) 730.
[4] N.G. Basov, Yu.A. Babeiko, V.S. Zuev, L.D. Mikheer, V.K. Orlov, I.V. Pogerelskii, D.B. Stavrovskii, A.V. Startser and V.I. Yalovoi, Soviet J. Quantum Electron. 6 (1976) 505; I.S. Datskevich, V.S. Zuev, L.D. Mikheer and I.V. Pogoreslkii, Soviet J. Quantum Electron. 8 (1978) 831.
[5] J. Xu, D.W. Setser and J.K. Ku, Chem. Phys. Letters 132 (1986) 427.
[6] A. Kvaran, A. Ludviksson, W.S. Hartree and J.P. Simons, Abstract, 9th International Symposium on Gas Kinetics, Bordeaux (1986).

[7] K. Johnson, R. Pease, J.P. Simons, P.A. Smith and A. Kvaran, J. Chem. Soc. Faraday Trans. II 82 (1986) 1281
[8] A. Kvaran, I.D. Sigurdardottir and J.P. Simons, J. Phys. Chem. 88 (1984) 6383.
[9] K. Johnson, J.P. Simons, P.A. Smith, C. Washington and A. Kvaran, Mol. Phys. 57 (1986) 255.
[10] M.F. Golde and A. Kvaran, J. Chem. Phys. 72 (1980) 434, 443.
[11] K. Tamagake, D.W. Setser and J.H. Kolts, J. Chem. Phys. 74 (1981) 4286.
[12] K. Johnson, A. Kvaran and J.P. Simons, Mol. Phys. 50 (1983) 981.
[13] D.H. Stedman and D.W. Setser, J. Chem. Phys. 69 (1978) 4357.
[14] L.A. Gundel, D.W. Setser, M.A.A. Clyne, T.A. Coxon and W. Nip, J. Chem. Phys. 64 (1976) 4390.
[15] J. Balamuta and M.F. Golde, J. Chem. Phys. 76 (1982) 2430.
[16] S.R. Langhoff, J. Chem. Phys. 73 (1980) 2379.
[17] T.H. Dunning and P.J. Hay, J. Chem. Phys. 66 (1977) 3767.
[18] D.G. Hopper, A.C. Wahl, R.C.C. Wu and T.O. Tierman, J. Chem. Phys. 65 (1976) 5474.
[19] P.J. Chantry, J. Chem. Phys. 51 (1969) 3369.
[20] T.H. Dunning Jr. and P.J. Hay, J. Chem. Phys. 69 (1978) 134.
[21] B.C. Lascowski, S.R. Langhoff and P.E.M. Siegbahn, Intern. J. Quantum Chem. 23 (1983) 483.
[22] K.P. Huber and G. Herzberg, Molecular spectra and molecular structure, Vol. 4, Constants of diatomic molecules (Van Nostrand Reinhold, New York, 1979).
[23] T.D. Dreiling and D.W. Setser, J. Chem. Phys. 75 (1981) 4360.